Available online at www.sciencedirect.com
ScienceDirect
J. Mater. Sci. Technol., 2010, **26**(4), 293-305.
JMST
www.JMST.org

• *Invited Review*

Recent Development of SOFC Metallic Interconnect

Junwei Wu[1,2,3] *and Xingbo Liu*[1,2]†

1) Mechanical & Aerospace Engineering Department, West Virginia University, Morgantown, WV 26506, US
2) National Energy Technology Laboratory, Morgantown, WV 26507, US
3) Department of Materials Science and Engineering, Shenzhen Graduate School, Harbin Institute of Technology, University Town, XiLi, Shenzhen 518055, China

[Manuscript received Feburary 26, 2010]

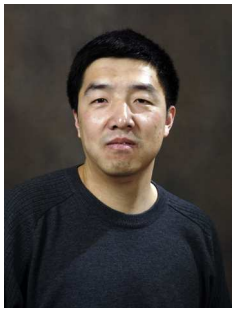

Dr. Xingbo Liu is an assistant professor in the Mechanical & Aerospace Engineering Department at West Virginia University, USA. He received his Ph.D in Materials Science from University of Science & Technology Beijing in 1999. Dr. Liu's current research focuses on high temperature materials for energy conversion, including superalloys and solid oxide fuel cells. He has received various awards, including the 2010 TMS Early Career Faculty Fellow Award.

Interest in solid oxide fuel cells (SOFC) stems from their higher efficiencies and lower levels of emitted pollutants, compared to traditional power production methods. Interconnects are a critical part in SOFC stacks, which connect cells in series electrically, and also separate air or oxygen at the cathode side from fuel at the anode side. Therefore, the requirements of interconnects are the most demanding, *i.e.*, to maintain high electrical conductivity, good stability in both reducing and oxidizing atmospheres, and close coefficient of thermal expansion (CTE) match and good compatibility with other SOFC ceramic components. The paper reviewed the interconnect materials, and coatings for metallic interconnect materials.

KEY WORDS: Solid oxide fuel cells (SOFC); Interconnect; Spinel; Coating

1. Introduction

Fuel cells are energy conversion devices that produce electricity directly from a gaseous fuel by electrochemical combination of the fuel with an oxidant. Solid oxide fuel cell (SOFC) technology has become increasingly attractive as a power generation method due to its low emissions, flexible fuel and high efficiency over traditional energy-conversion systems. The principal applications of SOFCs include: stationary power generation, auxiliary power unit (APU), and military applications. The high operating temperature, relative to other types of fuel cells, makes them ideal for combined cycle SOFC/gas turbine (GT) applications, and efficiency may approach 70–80%[1].

The fundamental mechanism of SOFC operation is the oxidation of hydrogen and other fuels at an anode and reduction of oxygen at a cathode to create a potential difference between two electrodes. The reaction products are water and CO_2, and the chemical energy of the reaction is liberated as electricity, as well as heat because of polarizations and ohmic losses[2]. A single SOFC is composed of electrolyte, anode and cathode. The electrolyte of SOFC is a solid, nonporous ceramic, usually Y_2O_3-stabilized ZrO_2 (YSZ). The SOFC operates at 600–1000°C where the ceramic electrolyte becomes conductive to oxygen ions, O^{2-}, but nonconductive to electrons. The high operating temperature has some advantages for minimization of polarization losses and fuel impurity tolerance effects[3,4]. Typically, the anode is made of nickel/

† Corresponding author. Prof., Ph.D.; Tel. +1 304 293 3339, Fax: +1 304 293 6689; E-mail address: xingbo.liu@mail.wvu.edu (X. Liu).

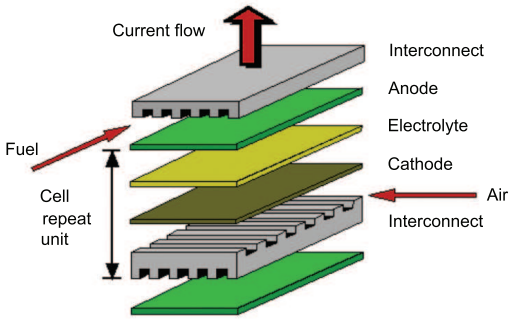

Fig. 1 Planar design for a solid oxide fuel cell (exploded view)

yttria-stabilized zirconia (Ni/YSZ) cermet and the cathode is electronically conductive perovskite Sr-doped $LaMnO_3$ (LSM) or other perovskite materials.

2. SOFC Interconnect

Single SOFC could only produce around 1 V open circuit potential (OCV). To generate a reasonable voltage, SOFCs are not operated as single units but as an array of units or "stack", with interconnects joining the anodes and cathodes of adjacent units. The flat-plate or planar type of SOFC, as shown in Fig. 1, has been the subject of intense research due to its potential for becoming an efficient, high energy-density power generation device[5].

Interconnects serve some vital functions in the SOFC stacks. They provide electrical connection between anode of one individual cell to the cathode of the neighboring one, and acts as physical barrier to avoid any contact between the reducing and the oxidizing atmospheres. The criteria for the interconnect materials are the most stringent of all cell components. In general terms, the interconnect has to meet the following demands[6,7,8]:

- Excellent electrical conductivity. The acceptable area-specific resistance (ASR) level is considered to be below 0.1 Ωcm^2;
- Adequate stability in terms of dimensions, microstructure, chemistry and phases at operating temperature around 800°C in both oxidizing and reducing atmospheres during 40000 h (service lifetime);
- Excellent imperviousness for oxygen and hydrogen to prevent direct combination of oxidant and fuel during operation;
- Thermal expansion coefficient (TEC) matching those of electrodes and electrolyte, around 10.5×10^{-6} K^{-1}, so that the thermal stresses developed during start-up and shut down could be minimized;
- No reaction or interdiffusion between interconnect and its adjoining components;
- Excellent oxidation, sulfidation and carbon cementation resistance;
- Adequate strength and creep resistance at elevated temperatures;
- Low cost, as well as easy to fabrication and shaping.

There are, in general, two approaches in developing interconnect materials for SOFCs, *i.e.* ceramics and metallic alloys.

3. Lanthanum Chromites as Interconnect

The traditional material used for the SOFC interconnect is lanthanum chromite ($LaCrO_3$) for high temperature applications (~1000°C). Firstly, this material exhibits a remarkable high electric conductivity under SOFC operating conditions compared with typical ceramics[9], and the conductivity could be improved significantly by doping with Mg, Sr, or Ca. Secondly, the melting point of $LaCrO_3$ is 2783±20 K, and the material could remain stable at both the cathode and anode environment[10]. Thirdly, average coefficient of thermal expansion (CTE) of $LaCrO_3$ is 9.5×10^{-6} K^{-1}, which is quite close to CTE of YSZ (10.5×10^{-6} K^{-1})[11].

By means of doping at A or B site, many properties of $LaCrO_3$ will be improved accordingly, which has been summarized in literature [12]. In terms of mechanical strength, magnesium doping is less effective than that of calcium and strontium, and the strengths of strontium-doped lanthanum chromite are generally better than those of calcium-doped lanthanum chromite. In terms of CTE, at the same dopant level, Sr doped $LaCrO_3$ (LSC) has higher CTE than Ca doped $LaCrO_3$, which makes LSC closer to YSZ. In conductivity, Ca doped $LaCrO_3$ is higher than doped by Sr; nevertheless, both of them are much higher than un-doped $LaCrO_3$. Regarding Cr evaporation, the activity of chromium oxide in $La_{0.84}Sr_{0.16}CrO_3$ (5.5×10^{-6}) is lower than that for $La_{0.79}Ca_{0.21}CrO_3$ (3×10^{-4}), indicating that strontium is more effective in reducing the chromium oxide activity.

On the other hand, certain weaknesses of $LaCrO_3$ are evident: (1) $LaCrO_3$ is a p-type semiconductor, and its conductivity decreases with decreasing oxygen partial pressure as lanthanum chromite becomes oxygen deficient[6]; (2) compared with typical engineering materials, lanthanum, being a rare-earth element, is expensive; (3) $LaCrO_3$ is a ceramic material, and processing methods are limited which results in limitations as to the geometry of interconnect that can be fabricated; (4) $LaCrO_3$ is difficult to sinter to a high relative density, so the processing of a hermetic $LaCrO_3$ layer is quite difficult, which is the most significant drawback.

To achieve full densification, several options can be considered: 1) conventional liquid-phase sintering process can be used to promote densification; 2) firing $LaCrO_3$ between Cr_2O_3 plates (sandwich configuration) in conjunction with fast heating and cooling schedule improves the densification process[7]. No doubt that added manufacturing complexity and cost are inevitably incurred. Because of these weaknesses

of $LaCrO_3$, significant research efforts have been made to find an alternative material.

4. Matallic Alloys as Interconnect

With the reduction of SOFC operation temperature to 600–800°C, metallic materials can be used to replace $LaCrO_3$ as interconnects because of its superior advantages compared with its high temperature counterpart[10,13]. (1) Metallic materials have high mechanical strength. The interconnect in anode supported SOFC, also acts as a mechanical support for ceramic parts, and constructional connection to the external inlets and outlets. In some case, interconnect has been designed with extra channels for distributing the gas in co-, cross- and/or counter-flow configurations. Traditional $LaCrO_3$ could not fulfill the requirement. (2) Metallic materials have high thermal conductivity, which could eliminate the presence of thermal gradient both along the interconnect plane and across the components. (3) Metallic materials have high electronic conductivity, therefore giving decrease in resistance of the cell increased output. (4) Ease of fabrication, low cost and readily available.

It should be pointed out that almost all the candidate alloys typically contain Cr and/or Al (Si is a third possibility, but much less used) to provide oxidation resistance by forming oxide scales of Cr_2O_3 and Al_2O_3, respectively. For the chromia formers, there should be enough chromium in the alloys to form a continuous oxide scale and to effectively provide oxidation resistance under SOFC operating conditions. The aluminum content in these alloys should be controlled at a minimum to avoid formation of a continuous alumina layer, considering the insulating nature of alumina scales[13].

4.1 Chromium based alloys

At temperature as high as 900–1000°C, chromium based oxide dispersion strengthened (ODS) alloys was specially used to replace $LaCrO_3$. A representative alloy is Ducrolloy (Cr-5Fe-1Y_2O_3) that was specifically designed by Plansee Company to match the thermal expansion coefficients of other SOFC components[7]. Some other chromium based ODS alloys include: Cr-5Fe-1.3La_2O_3, Cr-5Fe-0.5CeO_2, Cr-5Fe-0.3Ti-0.5Y_2O_3 and others.

The reason to choose chromium based (chromia formation) alloys is because chromia has high conductivity compared to other oxides[6,12]. However, due to its high chromium content, the chromium poisoning for cathode and excessive chromia growth are inevitable. Excessive grown chromia layer will cause spallation after thermal cycles. Apart from that, ODS alloys is more difficult and costly to fabricate. Since melting can affect the dispersion of the oxides, these techniques are powder metallurgy based and designed to produce near-net-shape components. For example, a powder metallurgy technique for directly producing sheets of interconnects has been reported, however, the cost of the alloy was still very high[14].

4.2 Fe-Cr-*based alloys*

To get a continuous chromia layer, the substrate alloy should have enough Cr content. The critical Cr content has been summarized in literature [13] that critical minimum Cr content is approximately 20%–25% in order to ensure the formation of a protective, continuous Cr_2O_3 scale. Note that low Cr content (5% and 10%) has also been used as interconnect, but the oxidation resistance was reduced significantly when lowering the Cr content[15,16]. Low Cr steels (<5% Cr) consist of nearly pure Fe oxide accompanied by internal oxide precipitates of Cr_2O_3 and/or $FeCr_2O_4$ spinels. With increasing Cr content the scales become richer in spinel and chromia, which is accompanied by a decrease of the scale growth rate. Nominal composition of Fe-Cr-based alloys is shown in Table 1[14].

Stainless steels are usually divided into four groups: (i) ferritic steels; (ii) austenitic steels; (iii) martensitic steels; and (vi) precipitation hardening steels[13]. Among them, usually the ferritic stainless steels are the most promising candidates for SOFC interconnect applications because of their body-centered cubic structure which makes the CTE quite close to that of other SOFC materials. In addition, the processing methods of this type of alloys are quite simple[17,18,19]. However, effect of substrate impurities, Si and Al, on the performance of the interconnect could not be neglected, especially silicon, which could form a continuous layer between substrate and scale. Pacific Northwest National Lab (PNNL) has systematically investigated the $(Mn,Co)_3O_4$ coated SUS430 alloy (∼0.5 wt pct Si), showing ASR will increase sharply at 4000 h due to the formation of continuous silica layer. Accordingly, SUS 441, with the addition of Nb and Ti based on SUS430, has also been tested. The results displayed that ASR is quite low even for bare metal, because Nb tied up Si to prevent formation SiO_2 layer at the scale/metal interface[20].

During SOFC stack operation, interconnect will face reducing environment on anode side and oxidizing one on cathode side. Therefore, exposure tests in air, to an H_2O+H_2 gas mixture simulating the anode side service gas, and to air/H_2 gas dual atmosphere simulating real operation condition have been carried out in various reports. In H_2+H_2O gas mixture, the chromia morphology is slightly modified and the adhesion of the scale is improved. In dual atmosphere, the scales formed in air contained iron-rich spinel or Fe_2O_3 nodules, which were not present in the alloys exposed to air on both sides. This suggests that the mobility of iron is accelerated by hydrogen at the anode side[14,21].

4.3 Ni-Cr-*based alloys*

Compared with Fe-Cr-based alloys, Ni-Cr-base al-

Table 1 Nominal composition of Fe-based alloys[14]

Alloy	Concentration/wt pct										
	Fe	Cr	Mn	Mo	W	Si	Al	Ti	Y	Zr	La
Fe-10Cr	Bal.	10	<0.02		<0.1						
1.4724	Bal.	13					1				
SUS 430	Bal.	16–17	0.2–1.0			0.4–1.0	≤0.2				
Fe-17Cr-0.2Y	Bal.	17							90.2		
1.4016	Bal.	17									
Ferrotherm (1.4742)	Bal.	17–18	0.3-0.7		0.8–0.9	0.9–1.0					
Fe-18Cr-9W	Bal.	18			9						
Fe-20Cr-7W	Bal.	20			7	0.3	0.6			0.3	
Fe-20Cr	Bal.	20	<0.02		<0.1					0.2	0.04
AL 453	Bal.	22	0.3			0.3	0.6	0.02			0.1
1.4763(446)	Bal.	24–26	0.7–1.5	≤0.05		0.4–1		<0.05			
FeCRMn(LaTi)	Bal.	16-25	?					?			?
Fe-Cr-Mn	Bal.	16-25	?								
Fe-25Cr-DIN 50049	Bal.	25	0.3		0.7		0.01				
Fe-25Cr-0.1Y-2.5Ti	Bal.	25						2.5	0.1		
Fe-25Cr-0.2Y-1.6Mn	Bal.	25	1.6						0.2		
Fe-25Cr-0.4La	Bal.	25									0.4
Fe-25Cr-0.3Zr	Bal.	25								0.3	
Fe26CrTiY	Bal.	26	0.1	<0.02		<0.05	<0.05	0.3	0.4		
Fe26CrTiNbY	Bal.	26	Composition not provided, but presumably same as Fe26CrTiY with Nb								
Fe26CrMoTiY	Bal.	26	0.1	2	<0.05	<005	0.3	0.3			
E-Brite	BAl.	26-27	≤0.1	1	0.03–0.2	≤0.05	≤0.05	≤0.01			
Al29-4C	Bal.	27	0.3	4	0.3		?				
Fe-30Cr	BAl.	30	<0.02		<0.1						

Table 2 Nominal composition of Ni-base alloys[14] for SOFC interconnect applications

Alloy	Concentration/wt pct									
	Ni	Cr	Fe	Co	Mn	Mo	Nb	Ti	Si	Al
Inconel 600	Bal.	14–16	6–9		0.4–1			0.2–0.4	0.2–0.5	0.2
ASL 528	Bal.	16	7.1		0.3			0.3	0.2	
Haynes R-41(Rene 14)	Bal.	19	5	11	0.1	10		3.1	0.5	1.5
Inconel 718	Bal.	22	18	1	0.4	1.9				
Haynes 230	Bal.	22-26	3	5	0.5-0.7	1–2			0.3	
Hastelloy X	Bal.	24	19	1.5	1.0	5.3				
Inconel 625	Bal.	25	5.4	1.0	0.6	5.7				
Nicrofer 6025HT	Bal.	25	9.5		0.1	0.5			0.5	0.15
Hastelloy G-30	Bal.	30	1.5	5	1.5	5.5	1.5	1.8	1	

loys always demonstrate better oxidation resistance and satisfactory scale electrical conductivity. To get a continuous chromia layer, only 15% Cr was needed to establish reasonable resistance to hot corrosion, which is lower than Fe-Cr-based alloys, and the optimum content was 18%-19%. Also, Ni based alloys are mechanically stronger. Nominal compositions of Ni-base alloy are shown in Table 2[14].

Most Ni-Cr-base alloys exhibited excellent oxidation resistance in moist hydrogen, growing a thin scale that was dominated with Cr_2O_3 and $(Mn,Cr,Ni)_3O_4$ spinels or Cr_2O_3[22]; therefore, it could be used as clad metal or plated layer in the anode side[23,24]. In air oxidation, high Cr containing alloys, such as Haynes 230 and Hastelloy S, formed a thin scale mainly comprised of Cr_2O_3 and $(Mn,Cr,Ni)_3O_4$ spinel during high temperature exposure; on the other hand, low Cr containing alloys, such as Haynes 242, developed a thick double-layer scale consisting of a NiO outside layer above a chromia-rich substrate, raising concern over its oxidation resistance for the interconnect applications[22].

The most significant problem to Ni-Cr-base alloys is potential CTE mismatch to cell components. To take fully advantages of the Ni-base alloys, novel designs of interconnects or stacks are necessary. The CTEs of Ni-Cr-based alloys containing W, Mo, Al, Ti were calculated using Eq. (1), a formulation derived for the CTE of Fe-free Ni alloys from room to 700°C:

$$\mathrm{CTE} = 13.9 + 7.3\times10^{-2}[\mathrm{Cr}] - 8.0\times10^{-2}[\mathrm{W}] - 8.2\times10^{-2}[\mathrm{Mo}] - 1.8\times10^{-2}[\mathrm{Al}] - 1.6\times10^{-1}[\mathrm{Ti}] \quad (1)$$

The bracketed terms in this equation represent the concentration (in weight percent, wt pct) of the specific alloying element. According to Eq. (1), most of the Ni-base alloys have higher CTE than that of other fuel cell components.

Table 3 Comparison of key properties of different alloy groups for SOFC applications

Alloys	Matrix structure	CTE×10^{-6}/K	Oxidation resistance	Mechanical strength	Manufactur-ability	Cost
CrBA	BCC	11.0–12.5 (RT-800°C)	Good	High	Difficult	Very expensive
FSS	BCC	11.5–14.0 (RT-800°C)	Good	Low	Fairly readily	Inexpensive
ASS	FCC	18.0–20.0 (RT-800°C)	Good	Fairly high	Readily	Inexpensive
FeBSA	FCC	15.0–20.0 (RT-800°C)	Good	High	Readily	Fairly expensive
NiBSA	FCC	14.0-19.0 (RT-800°C)	Good	High	Readily	Expensive

Jablonski and Alman from National Energy Technology Laboratory (NETL) have developed a new series of Ni-Cr-based alloys containing W, Mo, Al, Ti, *etc*, that potentially can be used as SOFC interconnect. After the test in moist air at room and elevated temperature for more than thousand hours, it was found that properties of alloy J5 were comparable to that of the commercial alloy Haynes 230. The nominal composition of J5 is Cr-12.5%, Ti-1%, Al-0.1%, Mo-22.5%, Mn-0.5%, Y-0.1%, Ni-balance[25].

4.4 Selection of metallic materials

To further define the alloy′s applicability as a SOFC interconnect, it was necessary to assess these alloys using relevant properties that correlate directly with the functional requirements of interconnect. These properties include: (i) CTE; (ii) oxidation and corrosion resistance; (iii) cost[13].

The coefficient of thermal expansion, was calculated from the displacement *vs* temperature data and is given in Eq. (2).

$$\alpha_{\mathrm{T}} = \frac{\mathrm{d}l/l_0}{\mathrm{d}T} = \frac{1}{l_0}\frac{\mathrm{d}l}{\mathrm{d}T} \tag{2}$$

where T is temperature in °C, l_0 is the length at room temperature, and l is the length at a given temperature. CTE has a strong relationship with the structure[13,26]. Body-centered cubic (BCC) structure has a lower CTE than face-centered cubic (FCC) structure[13]. The structures of metallic alloys are shown in Fig. 2[27].

In Wagner′s theory of oxidation, it is assumed that during the oxide growth, the transport of oxygen ions and/or metallic cations through the oxide scale takes place by lattice diffusion[13,28]. Thus the growth of the surface oxide scale follows the well-known parabolic law:

$$X^2 = Kt + X_0^2 \tag{3}$$

where X and X_0 is the thickness of the scale at time t and t=0, respectively; K is rate constant. It has been experimentally proved that the parabolic law of the growth of scale is valid for essentially all cases in which the scale is adequately thick and homogeneous[28].

Compared with all these results, ferritic stainless steel is the most promising candidate due to its low cost, good CTE match with YSZ, and good oxidation resistance. Comparison of key properties of different alloy groups[13,27] is displayed in Table 3.

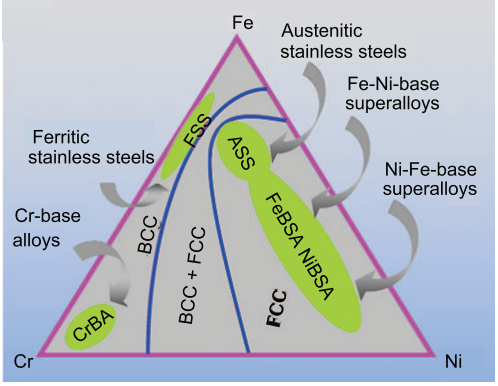

Fig. 2 Schematic of alloy design for SOFC applications[13,27]

4.5 Problems for metallic materials as interconnect

The application of ferritic stainless steel still poses many challenges even at reduced temperatures[7], which includes: (1) unacceptably high oxidation rate; (2) occurrence of buckling and spallation of the oxide scale when subjected to thermal cycling; (3) volatilization of high valence Cr-species in the form of CrO_3, or $Cr(OH)_2O_2$.

4.5.1 Excessive growth and spallation of oxide scale

Evaluation of oxidation behavior indicates that chromia scales on ferritic stainless steels can grow to micrometers or even tens of micrometers after thousands of hours′ exposure in the SOFC environment in the intermediate temperature range. Even without considering spalling and cracking, which are likely to occur, this scale growth would lead to an ASR increase and accompanying degradation in stack performance which are likely to be unacceptable. Use of optimized contact materials, such as a highly conductive oxide paste that is applied between the interconnect and cathode, can decrease the overall interfacial resistance[29]. However, as the thickness of scale keeps increasing, spallation will occur due to the increased thermal stress between coatings and substrate, or, in a severe case, loss of hermeticity of the interconnect layer. Figure 3 shows the SUS 430 scale spallation after 1900 h oxidation[30].

4.5.2 Chromium poisoning

The vaporization of chromium from the metal-

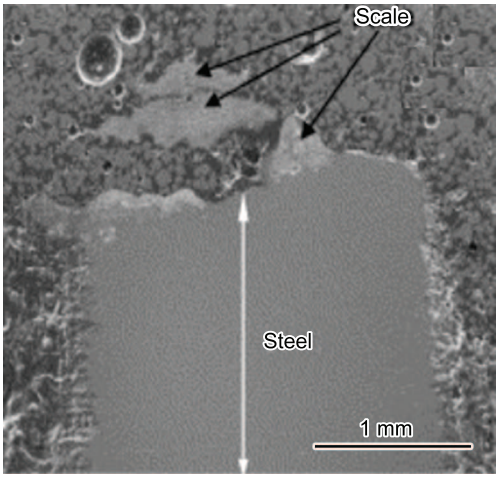

Fig. 3 SEM cross-section micrograph of uncoated UNS430 stainless steel rods after 1900 h oxidation in air at 800°C[30]

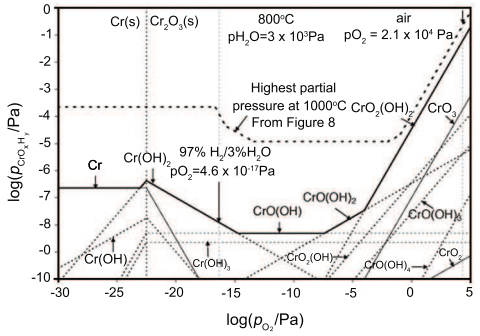

Fig. 4 Equilibrium vapor pressures of chromium-oxygen-hydrogen gas species at 800°C with a water vapor pressure of 3 kPa using thermodynamic data from Ebbinghaus[14]

lic interconnect can lead to severe degradation of the electrical properties of SOFC. This has been observed by different groups at the cathode side of SOFC using Cr_2O_3-forming alloys as interconnects with Y_2O_3-doped ZrO_2 as the solid electrolyte and LSM as the cathode[31–33]. It is based on the vaporization of Cr_2O_3 from interconnect surface as CrO_3(g) or $CrO_2(OH)_2$(g) as major gaseous species with chromium in the 6+ oxidation state. The equilibrium gas pressures for CrOxHy species as a function of oxygen partial pressure at 800°C is displayed in Fig. 4. The vapor pressure is becoming higher at higher oxygen partial pressure. Figure 5 presents temperature dependence of vapor pressure of different volatile chromium species. It is clear that $CrO_2(OH)_2$(g) shows the highest vapor pressure in the SOFC operation temperature range of 800–1000°C[14].

$$CrO_3(g) + H_2O(g) = CrO_2(OH)_2(g) \qquad (2)$$

Chromium-containing vapor species formed from

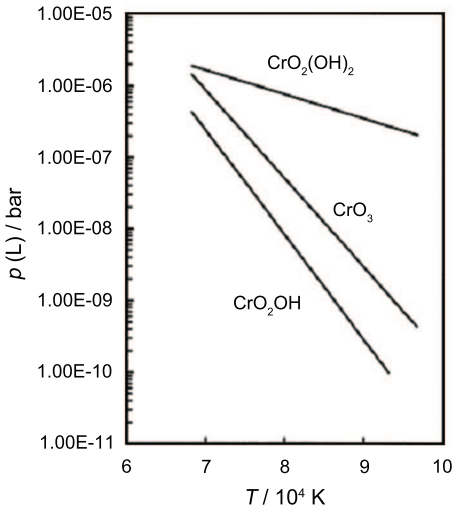

Fig. 5 Vapor pressures of different volatile chromium species as a function of temperature[14]

the interconnect material will electrochemically or chemically be reduced at the three-phase boundary {electrolyte/cathode/oxidant}. The resulting deposition can block the active electrode surface and degrade cell performance. The vapor pressures are higher in air so such poisoning is most likely to occur at the cathode. This degradation can be represented by a decrease in cell voltage or an increase (*i.e.* more negative) in cell overvoltage[14,34]. The schematic diagram of the Cr poisoning process is displayed in Fig. 6[35].

5. Interconnect Coatings

Recently, various coatings have been developed for metallic SOFC interconnect mainly to mitigate excessive chromia growth and chromium poisoning.

To qualify coating material as a viable, it should possess the following characteristics: (1) the diffusion coefficients of Cr and O in the coating should be as small as possible so that the transport of chromium and oxygen can be effectively hindered; (2) it should be chemically compatible and stable with respect to substrate, electrodes, seal materials and contact pastes; (3) It should be thermodynamically stable in both oxidizing and reducing atmospheres over the applied temperature range; (4) it must have low ohmic resistance to maximize electrical efficiency; (5) the thermal expansion coefficient should be well matched to the substrate so that the coating is resistant to spallation during thermal cycling[7].

5.1 Nitride coatings

Nitride coatings have been widely used in tools coatings due to their superior wear resistance. On the other hand, this type of coating could supply an alternative coating for SOFC interconnect applications due to their low resistance and high temperature

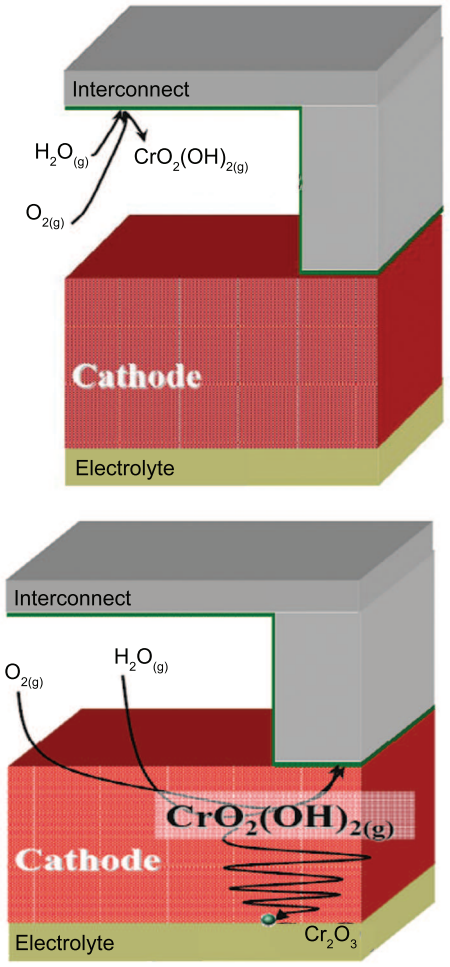

Fig. 6 Schematic diagram of $CrO_2(OH)_2$ formation and formation of Cr_2O_3 at the cathode and electrolyte interface[35]

stability[36].

Vacuum deposition, especially physical vapor deposition (PVD), has been widely used to prepare components and protective nitride coatings for SOFCs interconnect, due to the versatility of this technique as well as the ability to control composition and morphology[37]. Gannon *et al.* applied multilayer coatings consisting of repeated sections of CrN and a CrAlN superlattice[38]. The results showed that thinner bilayer (~1.1 nm) CrN/AlN superlattice coating are more favorable for the SOFC interconnect application than thicker 4.5 nm bilayer. Later, he deposited Cr-Al-O-N[39]. The introduction of oxide into nitride coatings reduces the Fe and Cr migration from substrate. Both of these results suggest PVD is an effective method to fabricate high quality coatings for metallic interconnects.

TiAlN with 30% and 50% Al[40] and SmCoN[41] coatings have been investigated in our group. Both of them revealed that nitride coatings could remain stable at 700°C, which is helpful to inhibit Cr and Fe migration from substrate. In addition,

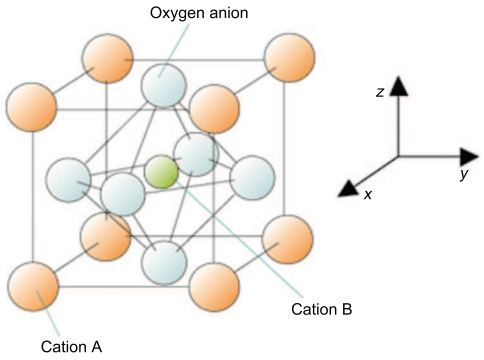

Fig. 7 Unit cell of a perovskite material

quite low ASR has been obtained in the short term test. However, these methods have limitations, such as high capital cost, low deposition rate. Most importantly, nitride is not quite stable at the temperature higher than 600°C.

5.2 Perovskite coatings

The structure of perovskite may be represented by the general formula ABO_3 where A is a lanthanide (such as La in most cases but sometimes Ce, Pr or Nd) and B a transition metal such as Co, Mn, Fe, Cr, Cu or V. Alkaline earth metals such as Sr, Ca or Ba can be substituted for sites A and a transition metal for site B[42]. The unit cell of perovskite is shown in Fig. 7[43]. For instance, the replacement of part of La^{3+} ions by Sr^{2+} can highly increase the electronic conductivity of perovskite in $LaCrO_3$, $LaMnO_3$ and $La(Co,Fe)O_3$.

$LaCrO_3$, traditional interconnect material, have been deposited by Orlovskaya *et al.* using r.f. sputtering[44]. It was found that two-step phase transformation occurred from as-deposited amorphous phase. The first step is from the X-ray amorphous state to a major intermediate phase: monoclinic $LaCrO_4$ monazite. A finite amount of La_2CrO_6 phase was also formed. The second step is the transformation of $LaCrO_4$ into the $LaCrO_3$ perovskite phase. During this transition only nanoporosity appears. These distinctive nanostructures have excellent potential for use as SOFC interconnect coating. Another option is to coat these alloys with an oxide layer that subsequently reacts with chromia to form a chromite (or chromate). Reactive formation of $LaCrO_3$ coating on SS-444 alloy *via* templated growth from thermally grown Cr_2O_3 and sputtered La_2O_3 layers has been demonstrated by Zhu *et al.*[45]. The results revealed that coated samples show much lower electrical resistance compared to the uncoated samples after similar thermal exposure for 100 h at 850°C. However, this approach suffers the obvious drawback of difficulty in controlling the composition of the reaction products. Therefore, coating with perovskite directly on the surfaces of the metallic interconnects

is preferred.

LSM has been widely used as SOFC cathode material. Due to its high electrical conductivity and thermal compatibility and stability in oxidizing environment, it has also been investigated as interconnect coatings. The presence of an LSM coating is crucial in maintaining the low level of contact resistance at elevated temperatures over extended periods of time. Slurry LSM coating was investigated on SUS430 substrate[46]. After sintering at 1200°C for 2 h in N_2, followed by heat treatment at 1000°C for 3 h in air, stable LSM-coated SUS 430 showed a low area-specific resistance (ASR) and maintained almost a constant value for 2600 h. Additionally, interactions between LSM coatings and RA446 were explored[47]. In the early 500 h, LSM could react with Cr diffused from substrate to form $LaCrO_3$, $(Cr,Mn)_3O_4$ and Cr_2O_3. The latter two phases have un-negligible Cr evaporation rates.

The reactions and complicated sintering process are originated from not fully dense coating and inherent porosity of perovskite, which could supply a path for Cr migration. It is necessary to deposit fully dense coatings to inhibit Cr diffusion and increase conductivity. Recently, perovskite coatings of LSM, LSCF were deposited by aerosol deposition, which is based on the impact adhesion of fine particles, and nearly 95% dense coatings could be obtained. After 100 h of oxidation at 800°C, area-specific resistance of LSM and Sr and Fe doped $LaCoO_3$ LSCF coated alloys was 20.6 and 11.7 $m\Omega \cdot cm^2$ respectively. And most importantly, no chromium was spotted in coatings by EDX line scan[48].

5.3 Spinels

Compared with perovskite, some spinels show better performance in preventing oxygen inward diffusion and Cr outward diffusion. However, the Cr evaporation is still a problem for Cr containing spinels. $MnCr_2O_4$ has been found as a product of reaction between chromium oxide and the Mn diffusion from Crofer 22 substrate, but the Cr evaporation is unnegligible. $CoCr_2O_4$ coatings cause no cell performance degradation in 1000 h test[49], and long term test is necessary to prove the coatings effectiveness.

Among all Cr-free spinels, $(Mn,Co)_3O_4$ spinel is considered the most promising candidate for the SOFC interconnect coatings. Previous work on Plansee Ducrolloy (Cr-5%Fe-1%Y_2O_3), indicated that a $(Mn,Co)_3O_4$ spinel layer could reduce chromium migration significantly, and predicted ASR at 10000 h is as low as 0.024 $m\Omega \cdot cm^2$ when using LSM and LSC contact paste[50]. Chen *et al.* reported $MnCo_2O_4$ coatings on the ferritic stainless steel AISI430 *via* slurry coating followed by mechanical compaction and air-heating[51]. Recently, Yang *et al.* at PNNL did a systematic study on $(Mn,Co)_3O_4$ spinel from conductivity, microstructure, CTE and long term ASR measurement of $(Mn,Co)_3O_4$ on ferritic stainless steel[52].

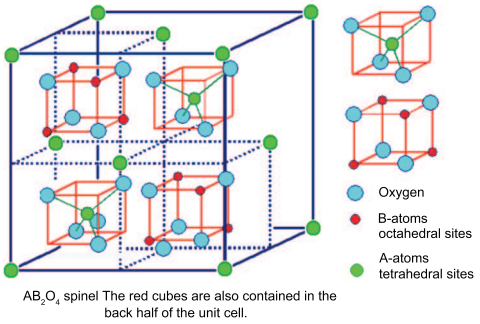

Fig. 8 Unit cell of spinel

5.3.1 Microstructure

The spinel structure consists of a close-packed oxygen lattice with cations in tetrahedral and octahedral positions. Half the octahedral sites and 1/8 of the tetrahedral sites are occupied in an ordered manner. The octahedral sites alternate between empty and filled. Unit cell of spinel is displayed in Fig. 8[53]. Lattice parameters lie consistently in the range from 0.805 to 0.850 nm. Cell size depends on the ionic radius and cation distribution. Spinels containing divalent manganese cations always have the largest cell volume because of its large ionic radius.

Among the various $Mn_{1+\delta}Co_{2-\delta}O_4$ spinel compositions, $Mn_{0.5}Co_{2.5}O_4$ (δ=−0.5) and $MnCo_2O_4$ (δ=0) exhibited a cubic spinel structure, with Mn sitting on octahedral interstitial sites and Co on both tetrahedral and octahedral interstitial sites in the face-centered cubic oxygen ion lattice. While $Mn_{2.5}Co_{0.5}O_4$ (δ=1.5) and Mn_2CoO_4 (δ=1.0) demonstrated a tetragonal spinel structure. When δ=0.5, the $Mn_{1.5}Co_{1.5}O_4$ spinel was a dual phase material, containing both the cubic and tetragonal phases[52,54].

During heating and cooling, the spinels $Mn_{1+\delta}Co_{2-\delta}O_4$ with δ in the range of 0.3–0.9, thus exhibiting a dual phase structure at room temperature, undergo a cubic ↔ tetragonal spinel phase transformation. High temperature XRD analysis on $Mn_{1.5}Co_{1.5}O_4$ found that the cubic↔tetragonal spinel phase transformation occurred around 400°C[52,54].

5.3.2 Conductivity

Spinels are generally believed to be conducted by hopping of charge between octahedral sites. Thus the presence of different valence states among octahedral cations is beneficial to conduction[55]. Many $Mn_{1+\delta}Co_{2-\delta}O_4$ spinels are good electrical conductors. For example, the electrical conductivity tests on the $Mn_{1.5}Co_{1.5}O_4$ spinel indicated an electrical conductivity of ∼60 $S \cdot cm^{-1}$ at 800°C in air, which is 2-4 orders of magnitude higher than Cr_2O_3 and $MnCr_2O_4$, as shown in Fig. 9. By comparison, the measured electrical conductivity of $MnCo_2O_4$ and

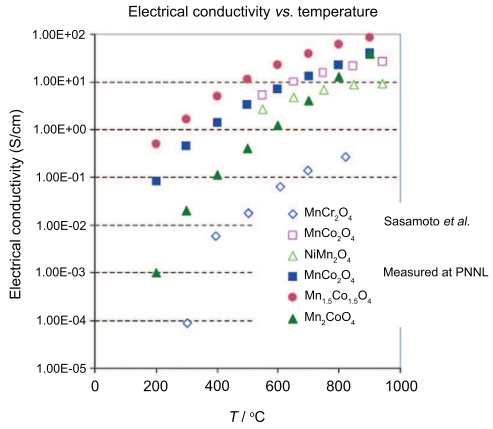

Fig. 9 Electrical conductivity of different spinels as a function of temperature

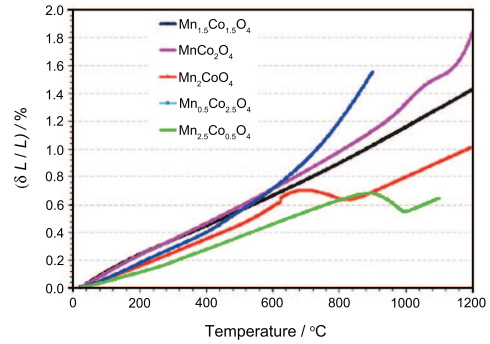

Fig. 10 Thermal expansion behavior of $Mn_{1.5}Co_{1.5}O_4$

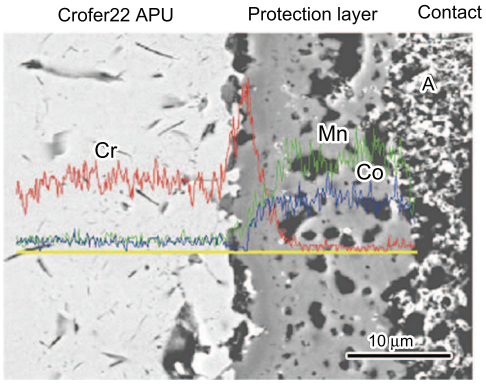

Fig. 11 Microstructural and compositional analyses on the $Mn_{1.5}Co_{1.5}O_4$ protection layer subjected to a contact ASR measurement for a period of 6 months under thermal cycling[52]

Mn_2CoO_4 (not shown here) was lower than that of $Mn_{1.5}Co_{1.5}O_4$ at 800°C in air[56].

5.3.3 CTE

The phase transformation always has appeared to have negligible effects on the thermal expansion behavior of the spinel material. As shown in Fig. 10, the thermal expansion of $Mn_{1.5}Co_{1.5}O_4$ exhibited a good linearity with temperature (11.5×10^{-6} K^{-1}, 20-800°C). In addition, the spinel demonstrated a good thermal expansion match to ferritic stainless steels such as Crofer 22 APU and AISI 430, as well as the perovskite cathode compositions such as $La_{0.8}Sr_{0.2}MnO_3$ and $La_{0.8}Sr_{0.2}FeO_{3.54}$[54,56].

Moreover, the CTE of $MnCo_2O_4$ is very close to that of $Mn_{1.5}Co_{1.5}O_4$ below 1000°C.

5.3.4 Cr retention capabilities

Recently, long term evaluation of $(Mn,Co)_3O_4$ spinel slurry coating has been carried out by Yang *et al.*[52,54]. After the 6 months and 125 thermal cycling tests, the coatings still adhere well to the substrate, and no spallation occurred. Further EDS linescan analysis of cross section revealed a sharp, thin Cr profile across the interface between the subscale and the spinel protection layer, with no chromium detectable in the spinel protection layer, as shown in Fig. 11.

Overall, it appears that the $(Mn,Co)_3O_4$ spinels are promising coating materials to posses high conductivity and CTE match with substrate, to reduce the scale growth, and to prevent chromium diffusion from the metal substrates.

6. Electrodeposition of Mn,Co Alloys with Following Oxidation

$(Mn,Co)_3O_4$ spinel has been applied to metallic interconnects materials by means of slurry coating[54], screen printing[52], and PVD[57]. Electroplating of alloys or individual metals followed by controlled oxidation and/or reaction to the desired phase may be a cost effective method for the formation of dense coatings. This method may also be more effective of applying coating on interconnects with complex geometries or even deposition on internal pores of foam materials.

6.1 Electrdeposition work from Literature

The deposition of alloys by simple elelctrodeposition method can only be accomplished when the deposition potential for each of the components are approximately the same[58,59]. However, the reduction potentials of the Co^{2+}/Co is $-0.28V_{SCE}$, whereas that of Mn^{2+}/Mn is more negative, $-1.18V_{SCE}$. This significant difference makes it impossible to obtain any Mn from conventional electrodeposition. Lowering the concentration of more noble metal (Co) in the electrolyte is one possible path, but it is not too practical for mass production. For instance, estimation of the concentrations necessary to bring the deposition potentials to equal levels for Mn^{2+} and Co^{2+} done using the Nernst equation and assuming dilute solutions (so that concentration can be used instead of activity) shows that the Co^{2+} concentration would need to be approximately 30 orders of magnitude more dilute

than the Mn^{2+} ion concentration.

To overcome this problem, different methods have been attempted previously. Christopher Johnson *et al.*[60] tried the two-step deposition processes of $Mn^{2+} \rightarrow HMnO_2^- \rightarrow Mn$.

$$\text{Step 1}: \ Mn^{2+} + 2H_2O \rightleftarrows HMnO_2^- + 3H^+ \qquad (4)$$

$$\text{Step 2}: \ HMnO_2^- + 3H^+ + 2e^- \rightleftarrows Mn(s) + 2H_2O$$

$$E^o = -0.163 \text{ V} \qquad (5)$$

The deposition potential of $HMnO_2^-$ is -0.163 V, much lower than -1.180 V for the Mn^{2+} species. The solubility product constant (K_{sp}) of the step 2 reaction at 50°C is 6.59×10^{-19}. Thus under typical conditions of $MnSO_4$ solution, the $HMnO_2^-$ concentration is very low and despite the lower E° value for this species the deposition potential remains high because of the low concentration. The concentration of $HMnO_2^-$ species can be adjusted at a number of pH values by using the equilibrium equation.

Anodic deposition of nanocrystalline Mn-Co-O coatings has been done by Weifeng Wei *et al*[61,62]. Because Mn has higher affinity to oxygen, and the low dissociation constant (K_d) of cobalt sulfate heptahydrate in solution, diluted Mn solutions were attempted to get coatings with different Mn/Co ratios. Eventually in solution of Mn:Co=29:1, it is possible to obtain coatings with Mn=18.7%, Co=19.0%, O=62.3%. Additionally, Co and Mn bi-layer deposition in two baths was done by M. Reza Bateni and co-workers[63].

In the past, electrodeposition of Mn/Co alloys has been carried out by S.S. Abd El Rehim and co-workers[64] as cathodic protective coating. We have attempted to repeat the experiments, but are not successful and other literature gave different summary about the Mn percentage change with current density[65]. On the other hand, some other researchers used very dilute more noble metallic salt solutions, which is only practical for lab experimental.

6.2 Mn/Co *alloys electrodeposition in our greup*

Constant current mode has been widely used for depositing single metal or alloys. For Mn/Co alloys co-deposition, it is unavoidable to have proton reduction and water splitting reactions. The total reactions occurring during Mn/Co cathodic deposition were shown as[66]:

$$2H^+(aq) + 2e \rightarrow H_2 \qquad (6)$$

$$Co^{2+}(aq) + 2e \rightarrow Co(s) \qquad (7)$$

$$2H_2O + 2e \rightarrow H_2 + 2OH^- \qquad (8)$$

$$Mn_2 + (aq) + 2e \rightarrow Mn(s) \qquad (9)$$

In the deposition, Sodium gluconate (gluconate) was added to the solution as chelating agent, $(NH_4)_2SO_4$ and Boris acid as pH buffer. All solutions are prepared by using deionized (DI) water.

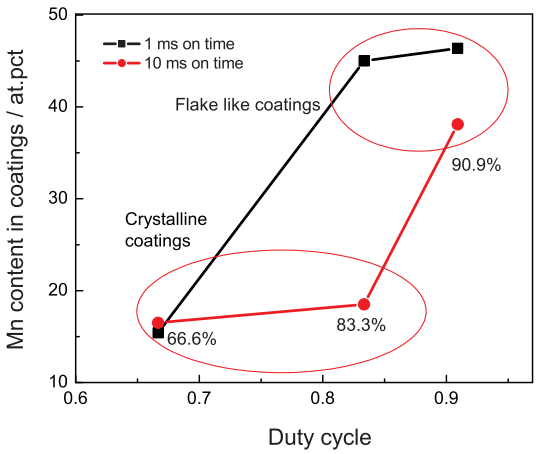

Fig. 12 Coatings composition changes with different duty cycles at 1 ms and 10 ms on time

Pulse plating has been regarded as better plating mode than DC plating. Three parameters, the peak current density, the on-time and the off-time can be varied independently. Higher peak current density than DC is applied to get higher over potential and more nucleation sites, which in dc lead to rough, powdery deposits. Off time in pulse plating enables larger currents/voltages to be applied during the on time, the mass transfer limitation can be alleviated and resulting surface morphology and current efficiency are improved. A review of the theory and practice of pulse plating is available[67]. By varying the on and off time, nano-crystalline alloys and multilayer coatings have been deposited successfully[68,69]. There are two important parameters concerning pulse plating, average current density i_a (Eq. (10)) and duty cycle γ (Eq. (11))

$$i_a = (i_p \times t_{on})/(t_{on} + t_{off}) \qquad (10)$$

$$\gamma = t_{on}/(t_{on} + t_{off}) \qquad (11)$$

Pulse plating was carried out at the on time of 1 ms and 10 ms, with the off-time of 1/10, 1/5 and 1/2 of the corresponding on-time[70]. The flake like and porous structure of the coatings at 1 ms on, 0.1 ms off and 0.2 ms off, and 10 ms on 0.1 ms off are demenstrated. With the increase of off-time, the morphology turns into compact coatings, which are characterized by regularly shaped crystalline grains, with apparent grain size ranging from 1 to 3 μm. EDX results shows stronger substrate peaks than the coatings of crystalline structure, which illustrated thinner coatings of flake like structure (not shown here). The composition of coatings was exhibited in Fig. 12. The flake like structure shows higher Mn content than that of crystalline coatings.

The oxidized coating was exposed to 800°C for 1200 h and ASR was measured. The ASR profile is shown in Fig. 13. During the initial 165 h, ASR value is not stable, probably due to the contact problem

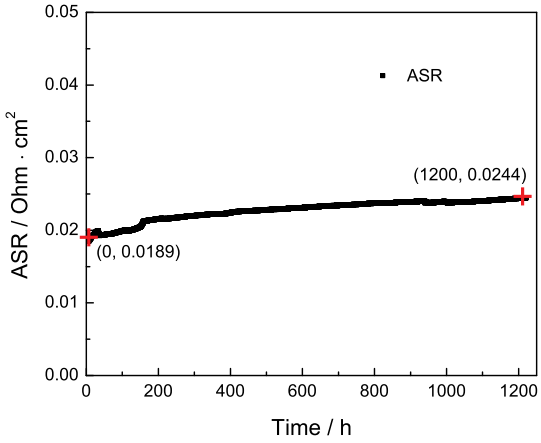

Fig. 13 ASR results for the Mn-Co coated T430 stainless steel[70]

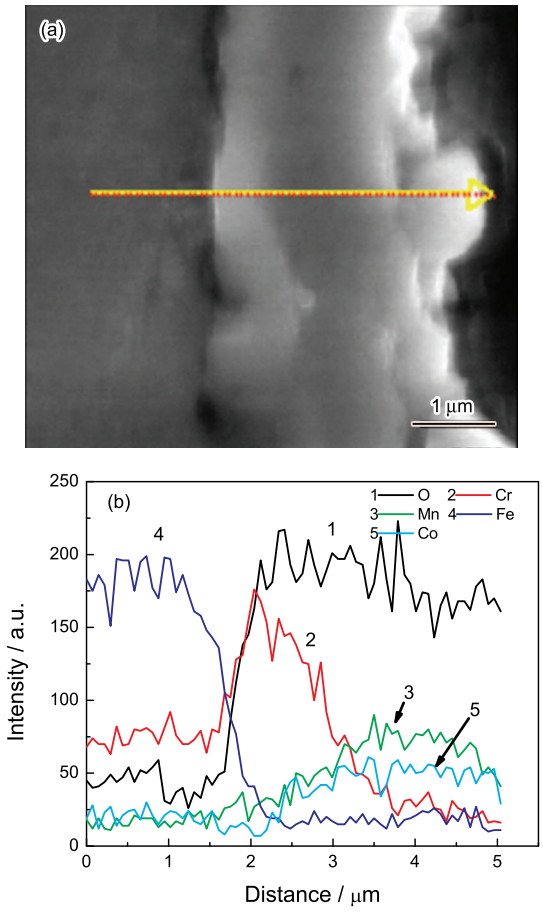

Fig. 14 (a) crosssection SEM morphology and (b) EDX linescan of Mn/Co coating after 1200 h ASR test[70]

between platinum paste and sample. Then it remains stable during the following 1000 h with only a slight increase. According to the value obtained initially and at 1200 h, ASR value at 40000 h was predicted to be 0.0460 $\Omega{\cdot}cm^2$, assuming it follows parabolic law, which is much lower than the target value of 0.1 $\Omega{\cdot}cm^2$ after 40000 h operation[6].

Cross-section of the coating shows dense, compact

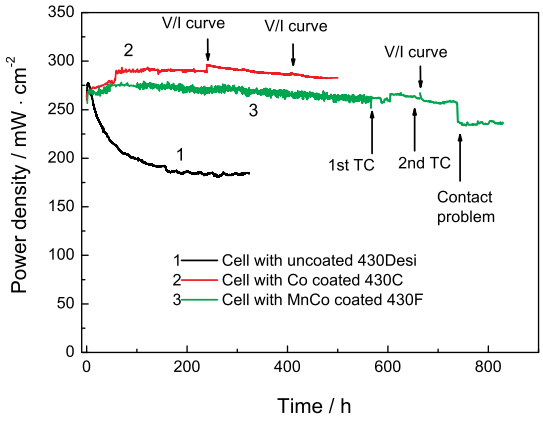

Fig. 15 Cell performances with interconnects as cathode current collectors

and good adhesion with the substrate, as exhibited in Fig. 14(a). Also there are some internal oxidation spots along the interface. EDX linescan profile demonstrates clearly that the coatings are composed of ~1.5 μm Cr_2O_3 interlayer and ~1.5 μm $(Mn,Co)_3O_4$ coating, as shown in Fig. 14(b). Note that Cr peaks remain quite low near the surface, which means little or no Cr diffuses into the coating surface.

Overall, the results have shown the possibilities of Mn/Co co-deposition. With the following oxidation process, spinels have been produced successfully[61,64].

Figure 15 shows the cell performance variation with time[71] at a constant current of 375 $mA{\cdot}cm^{-2}$. All cells show similar power densities at the beginning of the long-term tests, but different trends are evident. The cell with the uncoated interconnect was tested for 323 h. It shows slight improvement during the initial 3 h. The power then degrades rapidly during the following 100 h, and then slows down and reaches a plateau at ~200 h. No thermal cycle is conducted during the cell test. Compared with highest power density of 277 $mW{\cdot}cm^{-2}$, the total degradation rate is 33% in the initial 200 h.

The cell tested with the MnCo coated interconnect showed slight degradation from 50 to 735 h. At 735 h, the voltage suddenly dropped. This sudden decrease in cell voltage is believed to be the result of a voltage lead problem. In addition, at 566 h and 650 h, two thermal cycles occurred unintentionally at the same cell. After each thermal cycle, no performance drop was observed, suggesting that the Mn/Co coating adheres well to the steel substrate. The power density at 50 h is 275 $mW{\cdot}cm^{-2}$ and 258 $mW{\cdot}cm^{-2}$ at 735 h. The estimated degradation rate is 9% per 1000 h.

7. Summary

In spite of its advantages and large potential market, today there are two main obstacles to the commercialization of SOFC: materials costs and life

time[72,73]. Currently the materials cost for SOFCs is still too high for its widespread commercialization. In recent years, there have been tremendous progress on the development of both SOFC interconnect substrates and its coatings. However, various coatings have demonstrated their potential as the interconnect coatings due to their good oxidation resistance and chromium retention capability. However, similar to the other components in SOFC, the coatings are suffering from high cost and low long-term stability. Further development of the coating is needed in the future.

Acknowledgements

This technical effort was performed in support of the National Energy Technology Laboratory′s on-going research in solid oxide fuel cell Under the RDS contract DE-AC26- 04NT41817. The authors appreciate technical contributions from Drs. Christopher Johnson, Randall Gemmen, and Kirk Gerdes at NETL.

REFERENCES

[1] M.C. Williams, J.P. Strakey and W.A. Surdoval: *J. Power Sources,* 2005, **143**, 191.

[2] O. Yamamoto: *Electrochim. Acta,* 2000, **45**, 2423.

[3] S. Kakaç, A. Pramuanjaroenkij and X. Zhou: *Int. J. Hydrogen Energ.,* 2007, **32**, 761.

[4] F. Alcaide, P. Cabot and E. Brillas: *J. Power Sources,* 2006, **153**, 47.

[5] http://people.bath.ac.uk/cf233/sofc.html

[6] W.Z. Zhu and S.C. Deevi: *Mater. Sci. Eng. A,* 2003, **348**(1-2), 227.

[7] W.Z. Zhu and S.C. Deevi: *Mater. Res. Bull.,* 2003, **38**, 957.

[8] S. Fontana, R. Amendola, S. Chevalier, P. Piccardo, G. Caboche, M. Viviani, R. Molins and M. Sennour: *J. Power Sources,* 2007, **171**, 652.

[9] N. Minh: *J. Am. Ceram. Soc.,* 1993, **76**(3), 563.

[10] W. Vielstich, A. Hubert, M. Gasteiger and A. Lamm: *Handbook of Fuel Cells-Fundamentals, Technology and Applications; Fuel Cell Technology and Applications,* chapter 74, Wiley, New York, 2003.

[11] F. Tietz: *Ionics,* 1999, **5**, 129.

[12] J. Fergus: *Solid State Ionics,* 2004, **171**, 1.

[13] Z. Yang, K. Weil, D. Paxton and J. Stevenson: *J. Electrochem. Soc.,* 2003, **150**, A1188.

[14] J. Fergus: *Mater. Sci. Eng. A,* 2005, **397**, 271.

[15] S. Geng, J. Zhu, M. Brady, H. Anderson, X. Zhou and Z. Yang: *J. Power Sources,* 2007, **172**, 775.

[16] S.J. Geng, J.H. Zhu and Z.G. Lu: *Solid State Ionics,* 2006, **177**, 559.

[17] P. Piccardo, P. Gannon, S. Chevalier, M. Viviani, A. Barbucci, G. Caboche, R. Amendola and S. Fontana: *Surf. Coat. Technol.,* 2007, **202**, 1221.

[18] W. Qu, L. Jian, D. Ivey and J. Hill: *J. Power Sources,* 2006, **157**, 335.

[19] I. Antepara, I. Villarreal, L.M. Rodríguez-Martínez, N. Lecanda, U. Castro and A. Laresgoiti: *J. Power Sources,* 2005, **151**, 103.

[20] Z.G. Yang, G.G. Xia, G.D. Maupin, Z.M. Nie, X.S. Li, J. Templeton, J.W. Stevenson and P. Singh: *Advanced Interconnect and Interconnect/Electrode Interfaces Development at PNNL,* in 8th Annual SECA Workshop and Peer Review, San Antonio, TX, August 6-9, 2007.

[21] Z. Yang, M.S. Walker, P. Singh, J.W. Stevenson and T. Norby: *J. Electrochem. Soc.,* 2004, **151**, B669.

[22] Z. Yang, G. Xia and J. Stevenson: *J. Power Sources,* 2006, **160**, 1104.

[23] L. Chen, Z. Yang, B. Jha, G. Xia and J. Stevenson: *J. Power Sources,* 2005, **152**, 40.

[24] K.A. Nielsen, A.R. Dinesen, L. Korcakova, L. Mikkelsen, P.V. Hendriksen and F.W. Poulsen: *Fuel Cells,* 2006, **06**, 100.

[25] P. Jablonski and D. Alman: *Int J. Hydrogen Energ.,* 2007, **32**, 3705.

[26] B.C. Church, T.H. Sanders, R.F. Speyer and J.K. Cochran: *Mater. Sci. Eng. A,* 2007, **452-453**, 334.

[27] Z. Yang, G. Maupin, S. Simner, P. Singh, J. Stevenson and G. Xia: *6th SECA Annual Workshop,* Pacific Grove, CA April 18-21, 2005.

[28] K. Hauffe: *Oxidation of Metals,* Plenum Press, New York, 1965.

[29] P. Jian, L. Jian, H. Bing and G. Xie: *J. Power Sources,* 2006, **158**, 354.

[30] X. Deng, P. Wei, M. Bateni and A Petric: *J. Power Sources,* 2006, **160**, 1225.

[31] H. Yokokawa, T. Horita, N. Sakai, K. Yamaji, M.E. Brito, Y.P. Xiong and H. Kishimoto: *Solid State Ionics,* 2006, **177**, 3193.

[32] Y. Matsuzakiz and I. Yasuda: *J. Electrochem. Soc.,* 2001, **148**, A126.

[33] Y. Matsuzaki and I. Yasuda: *Solid State Ionics,* 2000, **132**, 271.

[34] J. Fergus: *Int. J. Hydrogen Energ.,* 2007, **32**, 3664.

[35] D. Liu, J. Almer, T. Cruses and M. Krumpelt: *ACerS 2007,* Coco Beach, FL, USA.

[36] S. Dey and S. Deevi: *Mater. Sci. Eng. A,* 2003, **324**, 58.

[37] L. Pederson, P. Singh and X. Zhou: *Vacuum,* 2006, **80**, 1066.

[38] P. Gannon, C. Tripp and A. Knospe: *Surf. Coat. Technol.,* 2004, **188-189**, 55.

[39] A. Kayani, R. Smith and S. Teintze: *Surf. Coat. Technol.,* 2006, **201**, 1685.

[40] X. Liu, C. Johnson, C. Li, J. Xu and C. Cross: *Int. J. Hydrogen Energ.,* 2008, **33**, 189.

[41] J. Wu, C. Li, C. Johnson and X. Liu: *J. Power Sources,* 2008, **175**, 833.

[42] F. Gaillard, J. Joly, A. Boréave, P. Vernoux and J. Deloume: *Appl. Surf. Sci.,* 2007, **253**, 5876.

[43] T. Ima, M. Sasaura, K. Nakamura and K. Fujiura: *NTT Tech. Rev.,* 2007, **5**, 1.

[44] N. Orlovskaya, A. Coratolo, C. Johnson and R. Gemmen: *J. Am. Ceram. Soc.,* 2004, **87**, 1981.

[45] J. Zhu, Y. Zhang, A. Basu, Z. Lu, M. Paranthaman, D. Lee and E. Payzant: *Surf. Coat. Technol.,* 2004, **177–178**, 65.

[46] J. Kim, R. Song and S. Hyun: *Solid State Ionics,* 2004, **174**, 185.

[47] Y. Zhen, S. Jiang, S. Zhang and V. Tan: *J. Eur. Ceram. Soc.,* 2006, **26**, 3253.

[48] J. Choi, J. Lee, D. Park, B. Hahn, W. Yoon and H. Lin: *J. Am. Ceram. Soc.,* 2007, **90**, 1926.
[49] C. Johnson, J. Wu, X. Liu and R.. Gemmen: *ASME Fuel Cell Conference*, New York, 2007.
[50] Y. Larring and T. Norby: *J. Electrochem. Soc.,* 2000, **147**, 3251.
[51] X.P. Hou, C. Jacobson, S. Visco and L.De Jonghe: *Solid State Ionics,* 2005, **176**, 425.
[52] Z. Yang, G. Xia, S. Simner and J. Stevenson:*J. Electrochem. Soc.,* 2005, **152**, A1896.
[53] http://www.tf.uni-kiel.de/matwis/amat/def_en/kap_2/basics/b2_1_6.html
[54] Z. Yang, G. Xia, X. Li and J. Stevenson: *Int. J. Hydrogen Energ.,* 2007, **32**, 3648.
[55] A. Petric and H. Ling: *J. Am. Ceram. Soc.,* 2007, **90**, 1515.
[56] J. Stevenson, Y. Chou, O. Marina, S. Simner, K. Weil, Z. Yang and P. Singh: *SECA Core Technology Program: Materials Development at PNNL,* SECA Core Technology Program Review Meeting, Lakewood, CO, October 25, 2005.
[57] V.I. Gorokhovsky, P.E. Gannon, M.C. Deibert, R.J. Smith, A. Kayani, M. Kopczyk, D. VanVorous, Z.G. Yang, J.W. Stevenson, S. Visco, C. Jacobson, H. Kurokawa and S.W. Sofie: *J. Electrochem. Soc.,* 2006, **153**, A1886.
[58] A. Brenner: *Electrodeposition of Alloys,* Academic Press, Vol (II), 1963.
[59] M. Paunovic and M. Schlesinger: *Fundamental of Electrochemical Deposition,* Wiley, 1998.
[60] C. Johnson, R. Gemmen and C. Cross: *Alloy Films Deposited by Electroplating as Precursors for Protective Oxide Coatings on Solid Oxide Fuel Cells Metallic Interconnect Materials,* MS′T 06 Conference, Cincinnati.
[61] W. Wei, W. Chen and D. Ivey: *Chem. Mater.,* 2007, **19**, 2816.
[62] W. Wei, W. Chen and D. Ivey: *J. Phys. Chem. C,* 2007, **111**, 10398.
[63] M. Bateni, P. Wei, X. Deng and A. Petric: *Surf. Coat. Technol.,* 2007, **201**, 4677.
[64] S.S. Abd El Rahim, M.A.M. Ibrahim and M.M. Dankeria: *Trans. IMF,* 2002, **80**, 105.
[65] J. Gong and G. Zangari: *Mater. Sci. Eng. A,* 2003, **344**, 268.
[66] J. Wu, Y. Jiang, C. Johnson and X. Liu: *J. Power Sources,* 2008, **177**, 376.
[67] J. Puippe and F. Leaman: *Theory and Practice of Pulse Plating,* AESF Soc, Orlando, FL, 1986.
[68] S.K. Ghosh, A.K. Grover, G.K. Dey and M.K. Totlani: *Surf. Coat. Technol.,* 2006, **126**, 48.
[69] K. Leistner, S. Fahler, H. Schlorb and L. Schultz: *Electrochem. Commun.,* 2006, **8**, 916.
[70] J. Wu, C. Johnson, Y. Jiang, R. Gemmen and X. Liu: *Electrichim. Acta,* 2008, **54**, 793.
[71] J. Wu, C. Johnson, R. Gemmen and X. Liu: *J. Power Sources,* 2009, **189**, 1106.
[72] S.P.S. Badwal: *Solid State Ionics,* 2001, **143**, 39.
[73] E. Ivers-Tiffée, A. Weber and D. Herbstritt: *J. Eur. Ceram. Soc.,* 2002, **21**, 1805.